

PAPER • OPEN ACCESS

Estimation of magnetic levitation and lateral forces in MgB₂ superconducting bulks with various dimensional sizes using artificial intelligence techniques








To cite this article: Shahin Alipour Bonab *et al* 2024 *Supercond. Sci. Technol.* **37** 075008

View the [article online](#) for updates and enhancements.

You may also like

- [Electromagnetic force behavior of superconducting bulks passing electromagnetic turnout](#)
Can Peng, Xuanbo Wang, Xucheng Zhou et al.
- [Investigation of saturation levitation force and optimization of permanent magnet guideway based on multi-seeded superconducting bulks model](#)
Wuyang Lei, Peiyu Yin, Yicheng Feng et al.
- [Increased levitation force in a stable hybrid superconducting magnetic levitation set-up](#)
P Bernstein, Y Xing and J G Noudem

Estimation of magnetic levitation and lateral forces in MgB₂ superconducting bulks with various dimensional sizes using artificial intelligence techniques

Shahin Alipour Bonab¹ , Yiteng Xing² , Giacomo Russo³ , Massimo Fabbri³, Antonio Morandi³ , Pierre Bernstein² , Jacques Noudem²  and Mohammad Yazdani-Asrami^{1,*} 

¹ CryoElectric Research Lab, Propulsion, Electrification & Superconductivity Group, James Watt School of Engineering, University of Glasgow, Glasgow G12 8QQ, United Kingdom

² NormandieUniv, ENSICAEN, UNICAEN, CNRS, CRISMAT, 14000 Caen, France

³ Department of Electrical, Electronic, and Information Engineering, University of Bologna, Viale del Risorgimento 2, 40136 Bologna, Italy

E-mail: mohammad.yazdani-asrami@glasgow.ac.uk

Received 5 March 2024, revised 14 May 2024

Accepted for publication 21 May 2024

Published 7 June 2024



CrossMark

Abstract

The advent of superconducting bulks, due to their compactness and performance, offers new perspectives and opportunities in many applications and sectors, such as magnetic field shielding, motors/generators, NMR/MRI, magnetic bearings, flywheel energy storage, Maglev trains, among others. The investigation and characterization of bulks typically relies on time-consuming and expensive experimental campaigns; hence the development of effective surrogate models would considerably speed up the research progress around them. In this study, we first produced an experimental dataset containing the levitation and lateral forces between different MgB₂ bulks and one permanent magnet under different operating conditions. Next, we have exploited the dataset to develop surrogate models based on Artificial Intelligence (AI) techniques, namely Extremely Gradient Boosting, Support Vector Regressor (SVR), and Kernel Ridge Regression. After the tuning of the hyperparameters of the AI models, the results demonstrated that SVR is the superior technique and can predict levitation and lateral forces with a worst-case accuracy scenario 99.86% in terms of goodness of fit to experimental data. Moreover, the response time of these models for the estimation of new datapoints is ultra-fast.

Keywords: extremely gradient boosting, kernel ridge regression, machine learning, magnesium diboride disc, magnetic guidance forces, modelling, support vector machine

* Author to whom any correspondence should be addressed.



Original content from this work may be used under the terms of the [Creative Commons Attribution 4.0 licence](https://creativecommons.org/licenses/by/4.0/). Any further distribution of this work must maintain attribution to the author(s) and the title of the work, journal citation and DOI.

1. Introduction

Nowadays, the applications of superconductivity involve energy, transportation, industry, medicine, communication, environmental protection, and various other aspects. With the advancement of superconductors like cuprates, MgB_2 , and iron-based superconductors, the utilization of bulk superconductors expands across various domains. These include magnetic field shielding, motors/generators, NMR/MRI, magnetic bearings, flywheel energy storage, and Maglev trains utilizing superconducting magnetic levitation (SML) systems [1–3]. While ReBCO bulk has received more attention for its superior superconducting properties and cost-effective cooling method in these applications, advancements in high-quality and large-size MgB_2 bulk fabrication [4–6] and two letters recently published in the “Superconductor Science and Technology” journal [7, 8] have unveiled the significant potential of MgB_2 bulk material for new applications such as SML and NMR systems utilizing hydrogen liquid cooling. This also presents a promising avenue for clean energy development [9]. Despite the operating temperature of MgB_2 is lower compared to cuprates like ReBCO, MgB_2 offers other advantages for the applications, including affordability, low density, reduced issues of anisotropy and inhomogeneity.

SML systems, benefiting from the flux pinning properties of bulk superconductors and requiring no energy supply except for system cooling, demonstrate a stable levitation force between the magnet source and the superconductor bulk [3]. It is noted that levitation stability is an aspect of paramount importance for real applications. Stable levitation occurs when, for a horizontal relative displacement between a superconducting bulk and a permanent magnet (PM) (typically one superconducting bulk and one conventional PM), a horizontal force in the same direction but opposite sign arises. This force, which is referred to as lateral force hereafter, helps to bring the two magnets (PM and cryomagnet) to the initial relative axial position, hence the levitation is stable. If the lateral force shared the same sign of the horizontal displacement, it would tend to make the magnet and the superconductor push each other away, resulting in an unstable levitation. The stability of such systems is closely related to the ratio of dimensions between the superconducting materials and the magnet source, the cooling distance, and the working temperature. A highly stable levitation force exceeding 400 N was achieved using a 120 mm diameter MgB_2 bulk fabricated within 2 h [8]. This value is comparable to systems consisting of ReBCO bulks [10], and the fabrication process for superconducting samples is much faster and simpler.

As the current research in the field is focused on finding the characteristics and conditions for superconducting bulk to yield strong and stable levitation, tackling this challenge exclusively experimentally would imply an enormous and expensive amount of work dedicated to the manufacturing of the superconducting samples and its experimental tests. The availability of reliable surrogate models for the calculation of the levitation and lateral forces produced with superconducting bulks would represent an efficient tool for guiding the research towards its current goals.

Artificial intelligence (AI) techniques have recently been the center of attention within superconducting community, as they can be used for optimization, estimation, condition monitoring, etc. AI techniques offer accuracies close to experimental measurement while their computation times are much less than modelling techniques such as finite element methods [11–14]. In addition, as AI techniques could help with prediction values for those data points which are not part of experiment or modelling campaign, they technically can provide interpolation and extrapolation with high accuracies [15, 16]; something that conventional statistical or mathematical methods are not capable of [17–19].

Recent advancements in AI have paved the way for significant breakthroughs in high-temperature superconducting (HTS) maglev technologies. Researchers are increasingly turning to AI and machine learning (ML) techniques to tackle complex challenges in design, diagnostics, and operational control of maglev systems [20]. A notable application of AI is in the development of neural network-based state observers designed to estimate system states and parameter matrices effectively. This approach includes the use of adaptive inversion control algorithms that incorporate output limitation characteristics to ensure stability against load variations and disturbances [21]. In the field of system diagnostics, AI has proven instrumental in vibration state detection. Backpropagation neural networks are employed to accurately detect and classify different vibration states within HTS maglev systems [22]. AI techniques like wavelet transform combined with neural networks facilitate the analysis of thermal-vibration correlations. This approach offers a non-invasive method to monitor internal temperature changes in superconductors, crucial for diagnosing system health and preventing failures before they occur [23].

AI's ability to handle complex problems extends to the prediction of levitation forces, a critical aspect of maglev technology. Aligning with [24, 25], where the authors utilize neural networks, such as back-propagation and gated recurrent unit models, to predict complex and nonlinear levitation and lateral forces, this study tries to implement robust AI techniques to develop intelligent models for prediction of these forces for MgB_2 bulks with various dimensional sizes.

In this paper, three AI algorithms that can manage various non-linear datasets with an extremely high accuracy, namely Extremely Gradient Boosting (XGBoost), Support Vector Regressor (SVR), and Kernel Ridge Regression (KRR) have been used to essentially estimate the levitation and lateral forces in MgB_2 superconducting bulks. These AI algorithms have been trained over a dataset containing the experimental results regarding the levitation and lateral forces between a conventional PM and MgB_2 bulks of diverse sizes and dimensions, and under different operating conditions (meaning the temperature of and the relative position the bulk). The findings of the work demonstrated that the AI models can estimate these forces with an accuracy of 99.86% of R-squared for testing dataset. Another major point about these models is that such an excellent accurate estimation is occurring in only milliseconds of time, making it suitable for fast predictions wherever is required. The MgB_2 samples, created

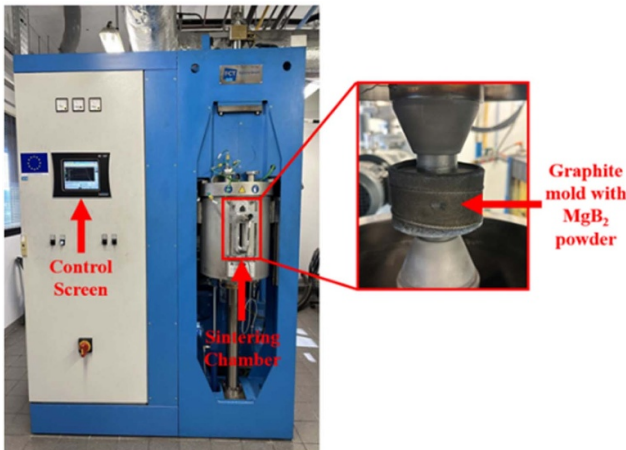


Figure 1. Photograph of spark plasma sintering equipment and the interior of the sintering chamber.

using the Spark Plasma Sintering (SPS) technology at the University of Caen-Normandy, were tested using a specific facility at the University of Bologna (UniBO), and the AI models were developed in the ‘Propulsion, Electrification & Superconductivity’ group at University of Glasgow specifically for these experimental data. The combination of the experimental data and AI models provides a more convenient and efficient method to identify suitable working conditions for the Superconducting Magnet Levitation System in the future.

In the following sections, first, the procedure of the tests, their findings, and data processing for AI modelling will be discussed. Next, in section 3, the algorithms of AI techniques and the performance indices that have been used in this paper will be explained. During section 4, initially the effective parameters of all three AI techniques will be presented and then the results of the sensitivity analysis on them are proposed. Finally, a conclusion based on the results of modelling will be presented.

2. Sample preparation and experimental testing

2.1. Sample synthesis and preparation

This study utilized ten cylindrical bulks of MgB_2 , prepared through the SPS technology [8] using MgB_2 powder acquired from Pavazyum company (in Turkey). SPS is renowned for its efficiency in producing highly dense MgB_2 bulks by applying uniaxial pressure and simultaneously high-intensity current to heat and densify the pellets [26, 27]. The powder is heated by the Joule effect, resulting in a typically faster process compared to other sintering methods [28]. Figure 1 shows the SPS machine (FCT Systeme GmbH, HD25, Rauenstein, Germany) located at the University of Caen-Normandy in the CRISMAT laboratory. The sintering of the samples occurred at 1150°C for 45 min with an applied axial pressure of 50 MPa under dynamic vacuum conditions (10^{-3} mbar). The samples shown in figure 2 typically exhibit a relative density exceeding 98%. Detailed information regarding the label name and dimensions of the fabricated MgB_2 discs can be found in table 1.



Figure 2. Photograph of the MgB_2 discs prepared by the spark plasma sintering.

2.2. Experimental setup

The levitation apparatus employed in this study was previously used and described in [29, 30]. This apparatus comprises a vacuum chamber that envelops a cooling copper plate designed to support the superconductor. Moreover, it includes a mechanical system for moving a PM and a set of probes for measuring the levitation and lateral forces. The displacement system consists of two stepping motors that can move the PM in both vertical (z -axis) and horizontal (x -axis) directions, being the directions along which the forces are measured. These motors are situated outside the vacuum chamber and are linked to the PM through a rod passing through a vacuum-tight flexible steel tube. The maximum excursion of the PM along the vertical and the horizontal direction is 55.9 mm, whereas levitation forces up to 700 N were recently measured in this facility [8]. The copper cold plate is linked to the second stage of the Sumitomo Cryocooler RDK 415D, potentially capable of cooling the plate down to 4.2 K with a cooling power of 1.5 W at the same temperature. However, during experiments, due to the input radiation the bulks in contact with the cold plate could reach 16 K at minimum. The superconductor’s temperature is regulated using four power resistors connected to the cold head and is monitored through two Si diodes. Pictures of the levitation facility are depicted in figure 3.

2.3. Experimental tests and data collection

The levitation and lateral force measurements were carried out after field cooling the superconductor within the field of a NdFeB PM with a diameter of 70 mm and a thickness of 35 mm. To measure the levitation forces, the magnet was positioned above the superconductor at a distance Z_{cp} (cooling height) from the sample’s surface, symmetrically aligned with the superconductor axis ($X = 0$). The MgB_2 disc was then cooled down to the measurement temperature (20 K). After the sample temperature stabilized, the magnet descended vertically toward the superconductor until it reached the minimum

Table 1. Parameters of fabricated MgB₂ samples.

Label	S1	S2	S3	S4	S5	S6	S7	S8	S9	S10
Diameter (mm)	69.5	65.2	59.6	49.7	50	50	50	50	50	56
Thickness (mm)	9.88	9.5	9.8	9.8	2	2.9	5	7.6	16	16.2

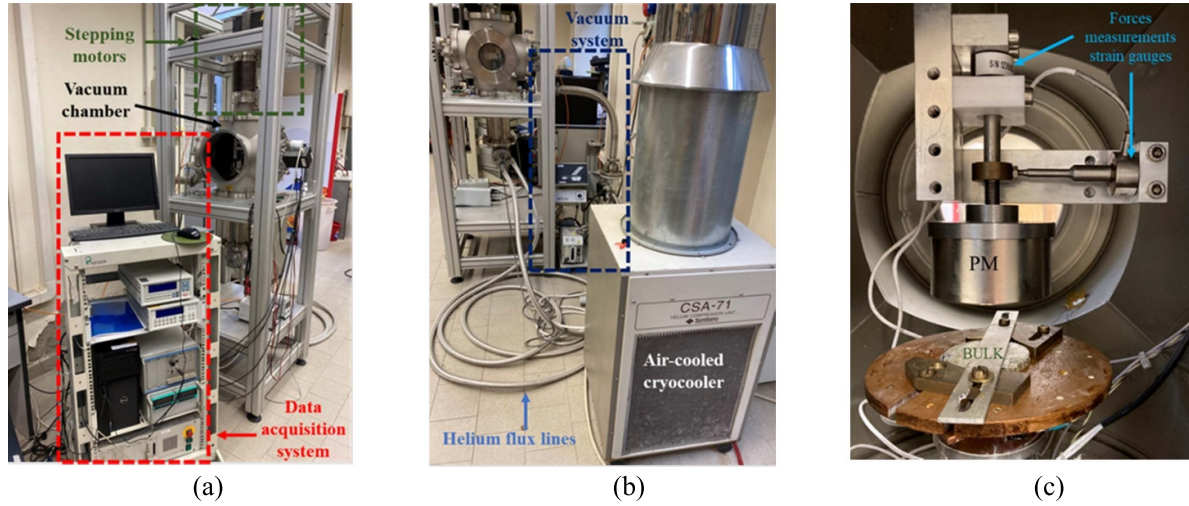


Figure 3. UniBO levitation apparatus pictures: (a) The motors of the displacement system, the instruments for acquiring measurements, and the vacuum chamber. (b) The cryocooler, the helium flux lines, and the vacuum system. (c) Inside of the vacuum chamber with the strain gauges, the permanent magnet and the superconducting bulk hold still by a copper and aluminium clamping system.

distance ($Z = Z_{\min}$) above the superconductor surface. At this point, the motion was reversed, and the magnet ascended to its initial position. The interaction force between the magnet and the superconductor was recorded as a function of the vertical distance (Z) between them throughout the entire process.

After the magnet returned to the cooling height, it was laterally moved along the surface of the MgB₂ disc until reaching X_{\max} . Then the motion direction was reversed and returned to zero. The vertical and lateral force was recorded as a function of X during this process. Furthermore, the distance between the magnet and the superconductor was systematically adjusted to different altitudes ($Z < Z_{cp}$), and the same measurements were carried out until reaching the point where the lateral force, F_x , exhibited a positive slope, indicating a loss of stability in the system [31].

The displacement speed of the magnet was maintained at 10 mm s^{-1} . Figure 4 shows the flow chart illustrating the entire force measurement process for all MgB₂ samples. Table 2 provides a summary of the experimental conditions utilized for different samples. Once the experimental campaign was completed, the data collected have to be processed to make it suitable for AI models, hence it was stored in a tabular form with proper labelling, in which each row contains one unique combination of experimental datapoints. In the resulting table, the columns contain the cooling point distance (Z_{cp}), the diameter of the bulk (D_{sc}), the height of the bulk (H_{sc}), the temperature of the bulk (T), the actual vertical distance between the bulk and the PM at the moment of the forces measurement (Z), the actual horizontal distance between the axes of symmetry of the bulk and the PM at the time of the forces measurement

(X), the movement orientation, and the lateral and levitation forces measured. For clearance, figure 5 offers a visual representation of the geometrical parameters mentioned earlier, while the first three rows of the dataset table (which contains 11 408 datapoints in total) are shown in table 3. It is reminded that Z_{cp} and Z refer to the vertical distance between the upper surface of the bulk and the lower surface of the PM.

For reaching the best possible AI prediction accuracy, it is decided to develop single target models, which means that, for a given combination of inputs, the model predicts only one type of quantity (either the levitation or the lateral force). Therefore, three types of tests are considered according to the aforementioned motivation: one that predicts the levitation force following a vertical movement along the shared axes of symmetry (#1), one that predicts the lateral force following a horizontal movement (#2), and one that predicts the levitation force following a horizontal movement (#3). Test #1 makes its prediction based on four inputs while for tests #2 and #3 seven inputs have been used. As an example, table 3 demonstrates the first dataset used for tests #2 and #3. Instead, the first test only needs four inputs, because no horizontal movement is implied in this case and also because the temperature was always kept equal to 20 K during the tests that explored the levitation force due to vertical movements of the PM. Details of the three considered tests are reported in table 4.

Once data is made as discussed, it is now ready for implementation in the AI algorithms; however, as the number of data is limited, it is common among the researchers that consider 80% of the data for training purposes of the network and 20%

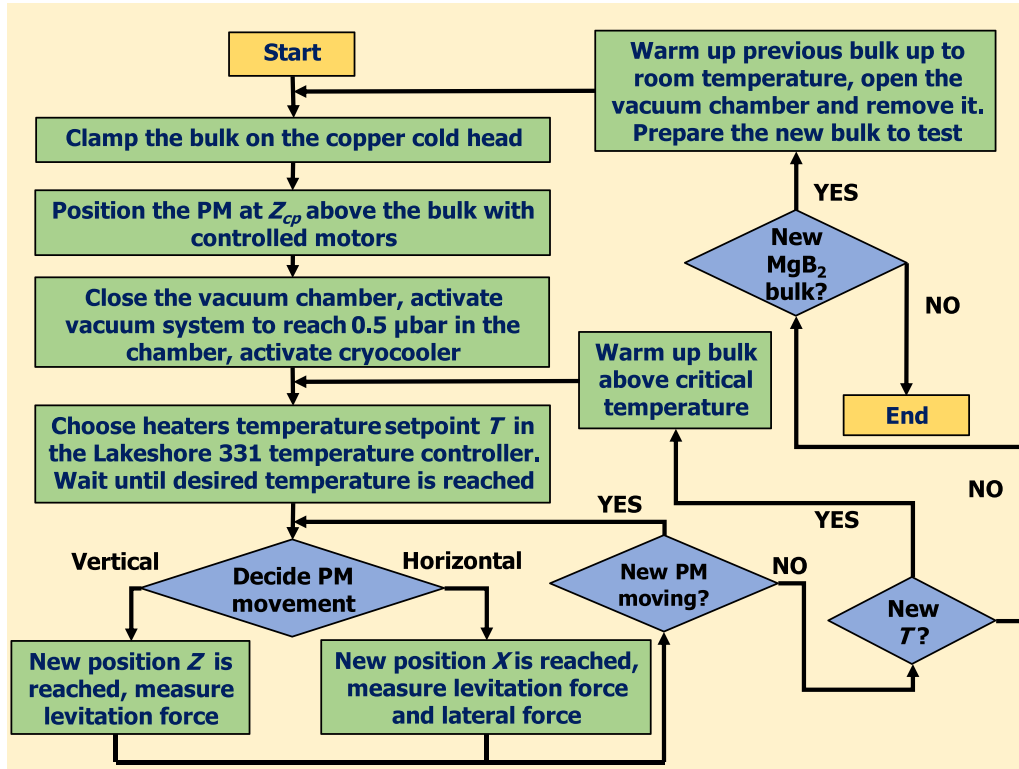


Figure 4. Flow chart of the whole force measurements.

Table 2. Experimental conditions for different samples.

Sample	S1	S2	S3	S4	S5	S6	S7	S8	S9	S10
Z_{cp} (mm)	25, 30, 35, 40, 50	30, 40, 50	30, 40, 50	30, 40	30, 40, 50	30, 40, 50	30	30, 40, 50	30	30
Temperature (K)	20	20	20	20	20	20	20	20	20	20, 26, 28, 29, 30

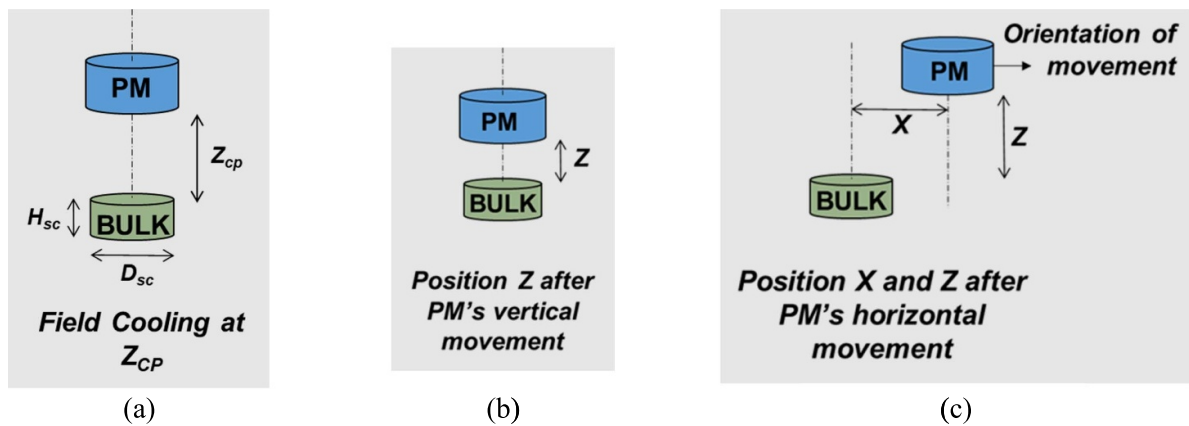


Figure 5. (a) Positions of the SC bulk (with diameter D_{sc} and height H_{sc}) and the PM during field cooling. During this time, the upper surface of the bulk and the lower surface of the PM are distance Z_{cp} from each other. The bulk is cooled down to temperature T . (b) After the bulk is cooled down and its temperature is stable, the PM is moved vertically to a new position Z . The bulk and the PM, still share the same axes of symmetry ($X = 0$), and the levitation and lateral forces are measured (waiting a few hundreds of milliseconds after the PM has stopped moving). (c) While the bulk temperature is stable and a vertical position Z is established, the PM is moved horizontally (according to a certain orientation, left or right) to a new position X , and the levitation and lateral forces are measured (waiting a few hundreds of milliseconds after the PM has stopped moving).

Table 3. A sample of pre-processed dataset.

Z_{cp} (mm)	D_{sc} (mm)	H_{sc} (mm)	T (K)	Z (mm)	X (mm)	Orientation of movement	Lateral force (N)	Levitation force (N)
30	49.7	9.8	20	6	1	Right	0.8	147.7
30	49.7	9.8	20	6	2	Right	0.6	147.5
30	49.7	9.8	20	6	3	Right	0.7	147.6
...

Table 4. Details of the input and output parameters of each test for implementation in the AI models.

Test	Input parameters	Output parameter	Movement orientation	Number of observations
#1	$Z_{cp}, D_{sc}, H_{sc}, Z$	Levitation force	Vertical	1416
#2	$Z_{cp}, D_{sc}, H_{sc}, T, Z, \text{Orientation of moving}, X$	Lateral force	Horizontal	11 408
#3	$Z_{cp}, D_{sc}, H_{sc}, T, Z, \text{Orientation of moving}, X$	Levitation force	Horizontal	11 408

of it for testing of the developed model. In this way, the predicted values of the model can be compared with experimental results, evaluating its performance and predictability.

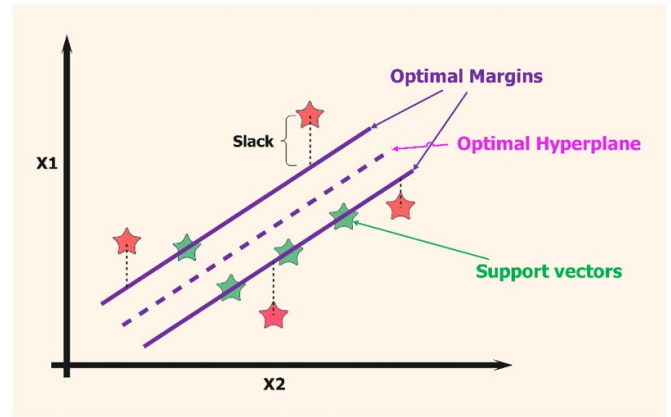
3. The proposed AI models

The selection of ML models in this study was driven by the imperative to utilize robust, versatile, and innovative approaches for the accurate estimation of both levitational and lateral forces. The rationale behind choosing these specific models can be explained as follows:

- These algorithms have demonstrated high levels of accuracy and efficiency in predictive tasks across various scientific fields. Their ability to deliver rapid predictions with high reliability is beneficial for real-time application in superconducting systems, where timely and accurate force estimations are critical. The literature provides numerous instances where these methods have been successfully applied in many engineering and scientific applications.
- The selection of these algorithms was also influenced by their unique features that cater to the specific requirements of our research. For instance, effective handling of outliers of SVR and scalability of XGBoost were key considerations. Also, the ability of KRR to handle multicollinearity effectively made it a suitable choice given the correlated nature of superconducting properties and external influences like temperature and magnetic field strength.

3.1. SVR

Support vectors are a family of ML methods including Support Vector Machine (SVM), which is used for classification, and SVR, which is for regression problems [32]. The main logic of the SVR is to convert the input dataset to a new dataset with higher dimensions. Then, it tries to simply find a hyperplane in the higher dimension space that best represents the relationship between the input and output features [33]. There are also two marginal lines, with same distance from the hyperplane and parallel to it. Although the ideal condition is that the hyperplane does not have any datapoint in the vicinity of it with marginal lines, in application there will be some points

**Figure 6.** Schematic of SVR method.

that are very close to it, which are known as support vectors [34, 35] and has been shown in figure 6. In this figure, X_1 and X_2 are two axes of higher dimensional space. Support vectors are the components that specify where and which orientation the hyperplane should be.

The main objective of the SVR technique is to maximize the marginal area around the hyperplane with respect to the tolerance that has been set for the algorithm to neglect support vectors. This can be reached by using the following equation [36]:

$$\text{Objective : Min } \left[\frac{\|w\|^2}{2} + C \left(v\epsilon + \frac{1}{P} \sum_{i=1}^P (\zeta_i + \zeta_i^*) \right) \right]$$

$$\text{Constraints } \begin{cases} f(x_i) - s_i \leq \epsilon + \zeta_i^* \\ s_i - f(x_i) \leq \epsilon + \zeta_i \\ \zeta_i, \zeta_i^* \geq 0 \\ \epsilon \geq 0 \end{cases} \quad (1)$$

In equation (1), $i \in \mathbb{N}$ and from 1 to P , term $\frac{\|w\|^2}{2}$ is known as the regularization factor, C is a constant for controlling the smoothness of model, v is a coefficient from 0 to 1 that controls the number of support vectors, ϵ is loss function, P is the total number of datapoints of the dataset that was used for training of the model, ζ_i, ζ_i^* are non-negative slack parameters, and $f(x_i)$ and s_i are predicted and actual value of x_i , respectively [37].

For high non-linear data, it is difficult (or impossible) to find a linear hyperplane for the data that can represent the data pattern with high accuracy. SVR is a method that uses kernel functions, which are also known as interpolation functions. By benefiting from this trick, the model can implicitly map the data into higher dimensions where it is easier to understand the pattern of data and therefore have an accurate prediction [38]. There are some kernel functions available in literature, but here we use three common ones, Linear, Polynomial, and Radial Basis Function (RBF). The mathematical form of these functions can be written as follows [39, 40]:

$$\text{Linear : } k(x_i, x_j) = x_i^T x_j + c_1 \quad (2)$$

$$\text{Polynomial : } k(x_i, x_j) = (x_i + x_j)^d \quad (3)$$

$$\text{RBF : } k(x_i, x_j) = \exp(-\gamma|x_i - x_j|^2). \quad (4)$$

In the equations (2)–(4), x_i and x_j are the input instances, γ is a positive random number or equal to $\frac{1}{2\eta^2}$ while η is the standard deviation of the population, d is the order of polynomial kernel, and c_1 is a constant. The effect of these functions on the accuracy of the model will be assessed in section 4.2.1.

3.2. XGBoost

XGBoost stands for eXtremely Gradient Boosting is a kind of ensemble technique that is well-known for its high accuracy of prediction and fast training process. Like any other ensemble ML technique, XGBoost uses the results of several decision trees (also referred to as boosting rounds) to make a more concise estimation [41]. This method which was first proposed by Chen *et al* [42] has the capability of handling both classification and regression problems. Generally, the predicted value for a regression problem can be evaluated through equation (5) [43]:

$$\hat{v}_i = \sum_{k=1}^K p_k(x_i), p_k \in T. \quad (5)$$

In this equation, k is the index of each of regression trees, $p_k(x_i)$ is the estimated value of k th regression tree for x_i , and T is the set of the regression trees. The goal of the XGBoost algorithm is to make the predictions as close as possible to the actual value by weighting the trees that have better accuracy and considering lower weight factors for the worse trees (see figure 7.)

In terms of mathematical equations, this goal can be written as:

$$\text{Objective} = \sum_{i=1}^n \text{loss}(v_i, \hat{v}_i) + \sum_{k=1}^K \Theta(p_k). \quad (6)$$

In equation (6), the first term is loss function, which evaluates the accuracy of the estimated value, and the second term is known as regularization factor and aims to avoid overfitting. Overfitting is a condition in which the model is too fitted to the trained data and understands all the fluctuations and noises

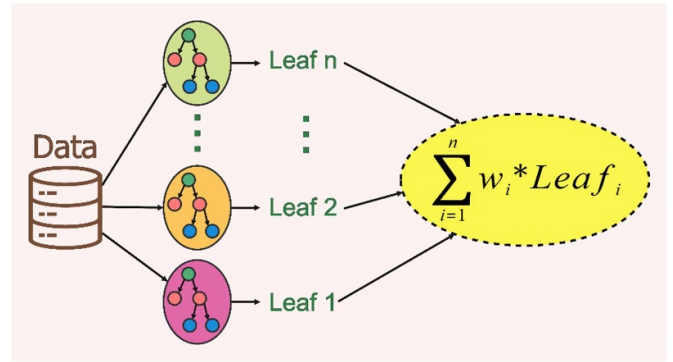


Figure 7. Schematic of XGBoost algorithm.

instead of the main trend. Considering \hat{v}_i^k as the estimated value of k^{th} regression tree, equation (6) can be rewritten as:

$$\text{Objective}^{(p_k)} = \sum_{i=1}^n \text{loss}(v_i, \hat{v}_i^{k-1} + p_k(x_i)) + \Theta(p_k) + c \quad (7)$$

where c is a constant. The regularization term also can be written as:

$$\Theta(p_k) = c_1 N + \frac{1}{2} c_2 \sum_{j=1}^N w_j^2. \quad (8)$$

In equation (8), the c_1 and c_2 are constants and w_j is the weight factor of j th leaf, where leaf refers to the results of one decision tree.

3.3. KRR

KRR is a ML technique in which utilizes a kernel for Ridge Regression algorithm to avoid overfitting [44] and performing a ridge regression in a higher dimensional space (like the general approach of SVR). But the difference is that this method uses squared error for updating of the results and finding the best regression while SVR uses a pre-set value for error. Like the other proposed methods, the model tries to optimize the predicted value through implementation of an objective function and minimizing of its value. As has been depicted in figure 8, the model has identified the pattern of datapoints (blue pentagons) and ignored the noises of the data where have significant different value from the overall trend of the data (red line).

This function can be written as follows [45]:

$$\text{Objective} = \frac{\sum_{n=1}^N (\alpha_n - \beta_n)^2}{N} + \sum_{m=1}^M \nu_m^2. \quad (9)$$

In equation (9), α_n is the actual value, β_n is the predicted value, N is the total number of samples (datapoints) of training dataset, M is the total number of effective parameters, and ν is a model parameter. Like the other methods, there is a regularization term in the KRR algorithm that does a trade-off between fitting to the input datapoints and avoiding overfitting. In this paper the same kernel functions that were listed

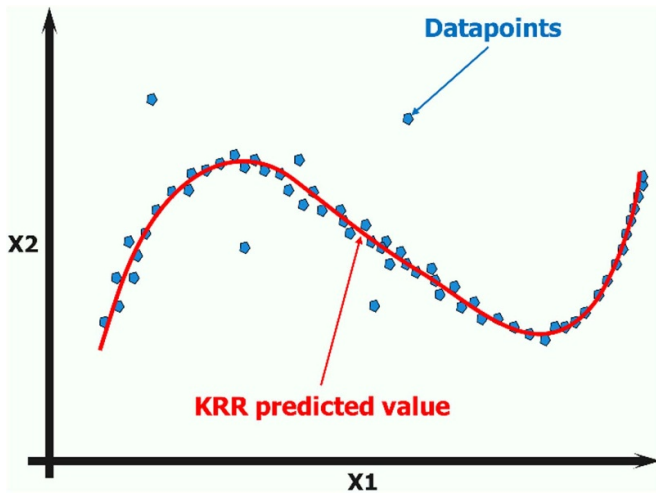


Figure 8. Schematic of KRR model.

in equations (2)–(4) are used for KRR algorithm too. More details on this method can be found on these papers [46–52].

4. Results and discussion

Now, the pre-processed dataset needs to be implemented into the ML models that were discussed in section 3. When it comes to developing an AI model, the learning curves are one of the most important tools that should be taken into consideration as they indicate how well a model learns from data over time or as the dataset size increases. A learning curve is a graph that compares the performance of a model on training and validation data over a varying number of training instances. It typically plots the training and validation error as a function of the training set size. It helps to distinguish between high bias (underfitting) and high variance (overfitting) problems by showing how the model performs on both the training set and a validation set as more data is used for training. It also provides insights into whether the model would benefit from more data (if the validation error continues to decrease with more data) or if the model complexity needs to be adjusted (if there is a persistent gap between the training and validation errors). As an example, the learning curve of the XGBoost model for test #3 have been provided in figure 9. As can be seen with figure 9, initially, with few data points, the model has a high validation error, indicating that it cannot yet generalize well. The training error is also high, which is normal in the initial learning phase. As more data is introduced to the model, both errors decrease, with the validation error decreasing significantly, which shows the model is starting to generalize better with more information. This trend continues until both curves saturate and do not change notably by adding more training data.

In the following, first, the controlling parameters that highly affect the performance of each of the AI models are described. These parameters are known as hyperparameter among the researchers and tuning of these parameters is unavoidable to reach the best performance of AI model. Then, the models are trained and tested using the same input dataset but the new

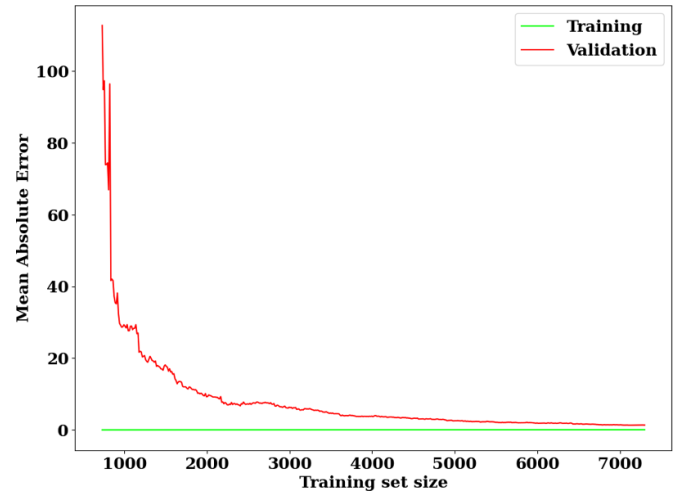


Figure 9. Learning curve of XGBoost model for test #3.

hyperparameters. Also, a detailed discussion based on the results of the tests is provided. Finally, the results of the tuned AI models are compared.

4.1. Performance metrics

In order to assess the performance of the trained AI models, there are some common indicators that can help on the understanding of how accurately the models can predict the levitation and lateral forces. One of the most useful tools for this purpose is Root Mean Squared Error (RMSE). The main reason behind using this index instead of directly evaluation of the error is that it enlarges the effect of error in the points where the error is massive by squaring of its value. This is while in simply Averaged Error (AE) there is no difference between the error of the points. By the help of scale analysis, as it appears from the equation (10), the RMSE has the same scale of actual value, which in this case is the force. So, it has a unit of force that in this paper is reported with $[N]$.

$$\text{Root mean squared error} = \left[\sum_{i=1}^N \frac{(\alpha_i - \beta_i)^2}{N} \right]^{0.5}. \quad (10)$$

In this equation the variables have the same meaning of equation (9).

Another important indicator is the Residual Value (RV), which is a helpful tool to understand how the model has learned the data pattern. In fact, RV is the difference between coefficient of determination (also known as R-squared or R^2) and its maximum value, which is 1. In this way, the performance of the models can better be understood and compared with each other. What makes RV an extremely important metric is that it shows the general inaccuracy of the model instead of directly presenting the error. In this way, it is not dependent to the scale and quantity of the data and merely assess the goodness of fit of the model to the actual data. Therefore, the RV can be evaluated by using equation (11).

$$RV = 1 - R^2 = \frac{\text{Sum of squares residual}}{\text{Sum of squares total}} = \frac{\sum_{i=1}^N (\alpha_i - \beta_i)^2}{\sum_{i=1}^N (\alpha_i - \bar{\alpha})^2} \quad (11)$$

where $\bar{\alpha}$ represents the average value of α .

Mean Absolute Deviation (MAD) is another useful indicator that is extremely helpful for stability assessment of the model. This index is used because the accuracy of the AI models is dependent on the selection of datapoints for training and testing process; however, the robust algorithms are not highly dependent on this factor and therefore their performance does not fluctuate a lot. Therefore, MAD is used to show how stable the model is and the lower value of it shows less dependency on train-test splitting process. The mathematical form of MAD can be written as follows:

$$MAD = \sum_{j=1}^T \frac{|p_j - \bar{p}|}{T}. \quad (12)$$

In equation (12), p_j refers to the performance (either RV or RMSE) of j th iteration of a model, \bar{p} is the average value of p , and T is the total number of iterations.

4.2. Sensitivity analysis for optimal hyperparameter tuning

All AI methods are characterized by hyperparameters that significantly impact the accuracy of the trained models. As a necessity of every AI modelling, these parameters must be tuned to reach the best performance possible for that algorithm. As these parameters are different for each of the applied methods, they are discussed in individual subsections and their results for each of the tests #1, #2, and #3 are presented.

It is worth noting that for reaching an optimum value for each hyperparameter the grid search approach is used. In this approach, initially, an effective range in which the accuracy of AI model is changing notably must be detected through a trial-and-error process. Then, by testing the models that are trained with different values of the hyperparameters in the detected range and comparing the performance of the models, an optimum value that resulted in highest accuracy is chosen. Next, the optimal value is then fixed and employed to determine the optimal values for the other hyperparameters.

4.2.1. SVR. As SVR is a method that uses kernel trick, as previously described. Naturally, the selection of kernel is crucial to reach the lowest inaccuracies and RV. By using the dataset relating to each of tests #1, #2 and #3, the type of kernel varies among the three options that was first introduced in section 3.1. Referring to the bar charts presented in figure 10, RBF has the lowest RV when compared to linear and polynomial kernels for all three tests.

Another major hyperparameter is the regularization parameter. The strength of regularization in the model is inversely proportional to this parameter [53]. It is a positive float number that can have any value but in a common way of analysis, it is considered to vary in a geometric sequence with

a common ratio of 10. Therefore, the numbers from 0.1 to 10 000 are considered for this step of analysis as there was no significant change in the accuracy of the model for a range above this value. The importance of the tuning of this parameter is determined by the fact that too much value for it can lead the model to an overfitting condition. As is depicted in figures 10(c) and (d), for test #1 a value of 10^4 of this parameter represents the highest accuracy while for tests #2 and #3 the optimum value is 10^2 as the diagram is almost saturated in that point.

The last hyperparameter that is analyzed for SVR method in this paper is epsilon [53]. The importance of epsilon is stressed by the fact that it is the most impactful parameter on the marginal area around the hyperplane. Generally, a greater value of epsilon enlarges the distance between margin lines and hyperplane and therefore exacerbates the error of model. Meanwhile, too little values of epsilon may result in an overfitting condition due to very low tolerance for errors. Therefore, it is crucial to assess the influence of this parameter on model's performance during modelling with SVR. Upon closer inspection of figures 10, 0.01 as an optimal value for epsilon resulted in the lowest RV and RMSE values for all three tests.

4.2.2. XGBoost. XGBoost as an ensemble method, has its own unique hyperparameters, which are mostly about controlling of the decision trees that it uses to reach a final decision.

One of the major hyperparameters is the number of boosting rounds. The greater number of boosting rounds usually leads to more robust models with higher accuracy. That said, too much boosting rounds results can lead to overfitting. Also, increasing of the boosting round soars the training time of the model. For these reasons, it is crucial to consider a reasonable number of estimators for the model. As it appears from figures 11(a) and (b), for tests #1 to #3 a value of 70, 490, and 490 are the best choices for the number of estimators as they resulted in the lowest RV and RMSE.

Another hyperparameter for this method is the maximum depth. As appears from its name, it controls the maximum depth of the decision tree that the model generates internally. As the model tends to go as deep as possible to grasp the relation between the parameters, if this action is exaggerated, there is a possibility of overfitting for the final model that over focuses on specific values. Now, using the tuned value for the number of estimators and using the same approach of tuning process of it, a sensitivity analysis on the maximum depth is done [54]. Noteworthy findings are represented in figure 11(c) show that beyond a maximum depth more than 4 there are no notable changes in RV. However, figure 11(d) depicts that for tests #2 and #3, RMSE value is lower when the maximum depth is set to 5, making it a better choice.

The learning rate is also an important parameter that influences the performance of the model significantly. More commonly among the researchers, a value between 0 and 1 is considered for this parameter. Greater values of learning rate allow the model to reach a decision faster and converge quicker. As a result, the model is trained in less time. However, in some cases, this can lead to a condition that the model is off the

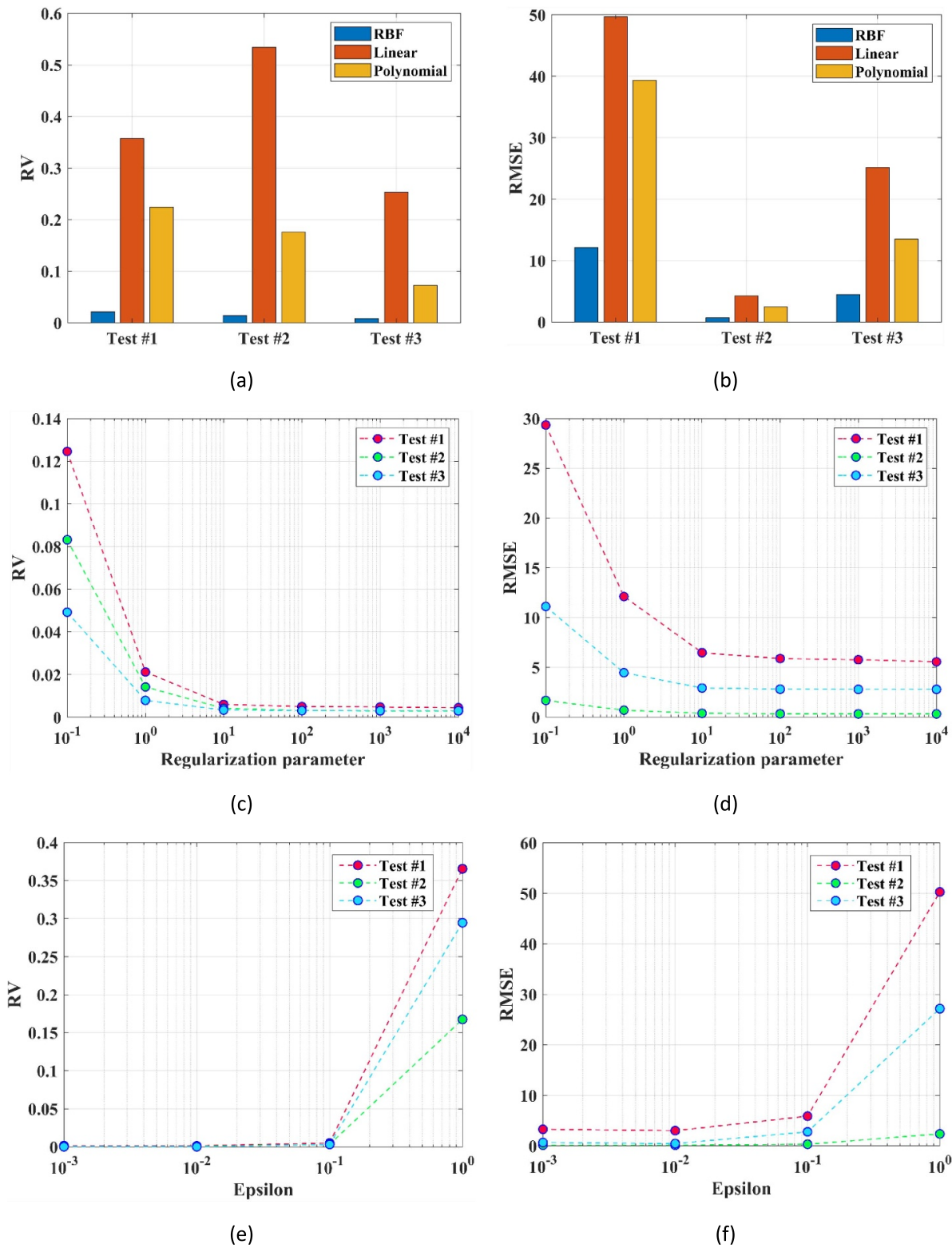


Figure 10. Tuning of the hyperparameters of SVR in terms of RV and RMSE for tests #1, #2, and #3.

course and does not converge (so the performance gets worse as the model trains more). A closer look at figures 11(e) and (f) illustrates how the performance of the models are changing as the learning rate varies. By considering RV and RMSE plots at

the same time, 0.35, 0.25, and 0.25 values of learning rate are chosen as the optimum values for tests #1 to #3, respectively.

It is worth noting that since the RMSE is an index that has the same unit as the predicted value, its value can be

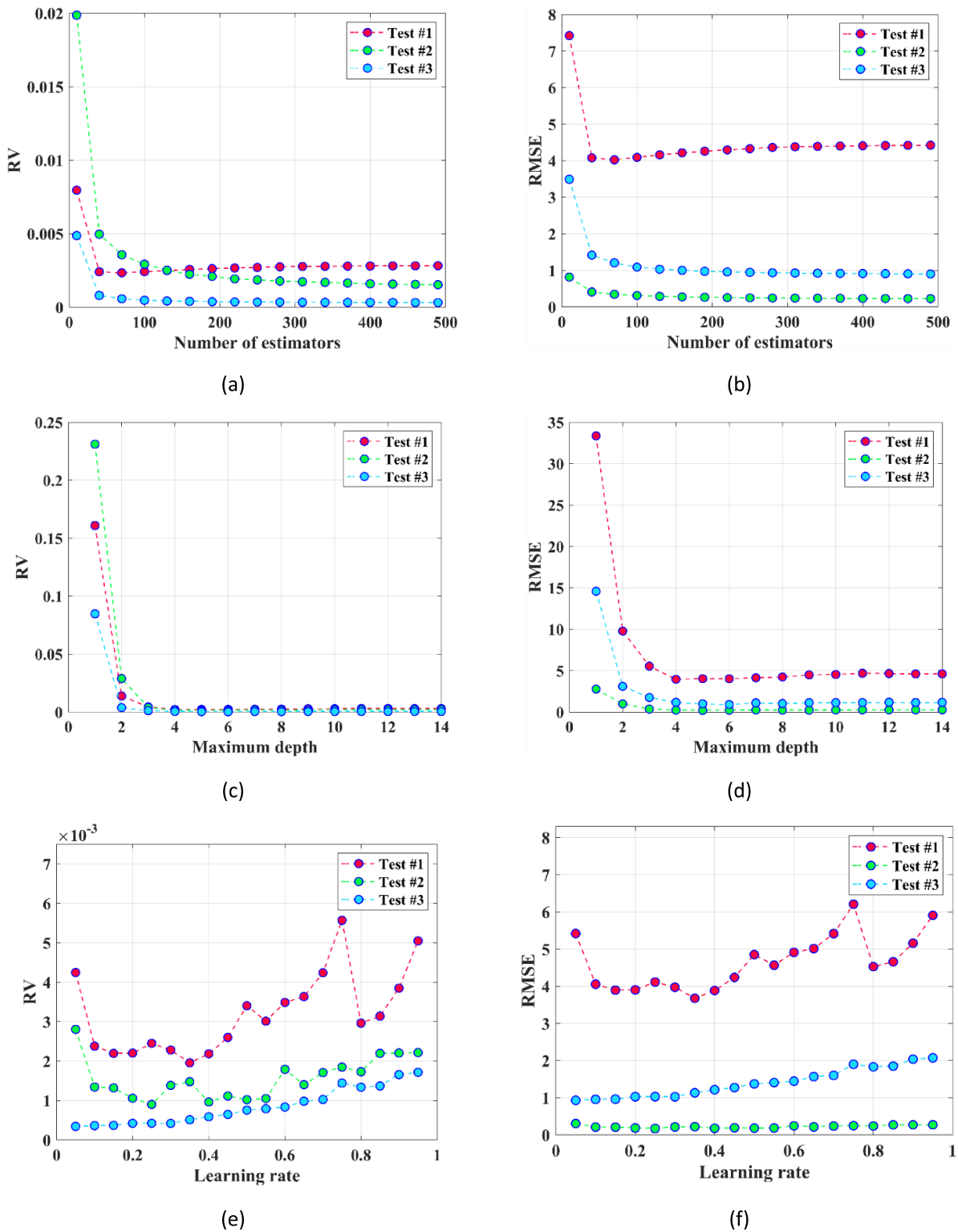


Figure 11. Tuning of the hyperparameters of XGBoost in terms of RV and RMSE for tests #1, #2, and #3.

higher or lower subject to the nature of the dataset. For instance, in this work, test #2 represents the data for lateral force, which is lower in magnitude than levitation force of test #3. Therefore, it generally has a lower RMSE than the model of test #3 (see figure 11). This is while the

RV of test #2 that represents the inaccuracy of the model is higher than test #3, meaning that the model of test #2 is less accurate than for test #3. This highlights how the RV is extensively important for assessment of the accuracy of a model.

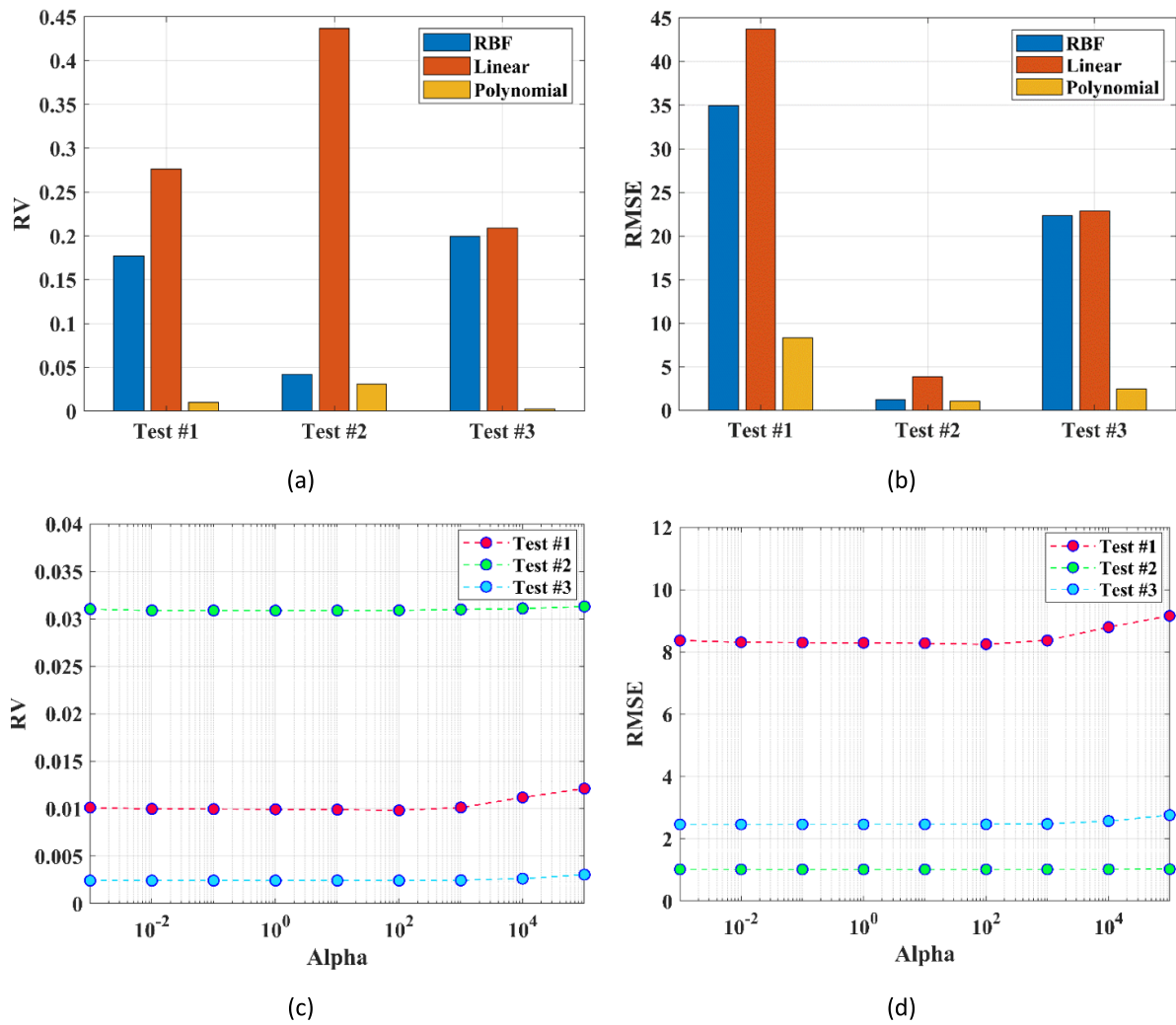


Figure 12. Tuning of the hyperparameters of KRR in terms of RV and RMSE for tests #1, #2, and #3.

4.2.3. KRR. The choice of kernel is of paramount importance during the modelling process with KRR. By varying the kernel between the same kernel options of SVR and comparing with the results of the testing of the models (figure 12), it can be found that Polynomial function is the kernel can yield the highest accuracy for the model.

Another crucial factor is the parameter that is usually referred to as alpha parameter. In fact, alpha is a parameter that controls the strength of the regularization term. Most commonly, its value α is varied exponentially of base 10 (like 0.01, 0.1, 1, ...). In this paper, for the purpose of sensitivity analysis of this parameter, it is considered to change between 0.001 and 1. With reference to figure 12, it can be observed that for tests #1 to #3, the value of 1, 100, and 0.001 for alpha results in the lowest RV and RMSE, respectively.

The summary of the best values of the hyperparameters for all methods within their testing range have been gathered in table 5.

4.3. Comparison of results and discussion

In order to establish which model performs the best, a comparison of RV of different methods is not sufficient and demands careful examination of the stability of the models. As the accuracy of estimation for AI methods is dependent on the quality and consistency of the training and testing data, stability of results that is a fundamental step in the AI modelling, warrants the reproducibility and repeatability of the results of the work. To reach this matter, the tuned models for all three AI algorithms undergo an iterative study where the randomized selection of datapoints for training and testing varies 50 times. In this way, it is ensured that the models with the reported performance are reproducible. After that, the mean and MAD values of RV, RMSE, and response time for all the models must be compared. It should be noted that the response time is dependent on the specification of the computer and can change device to device. The testing computer for this work has a 11th Gen Intel(R) Core(TM) i5-1135G7 @ 2.40 GHz CPU, 12 GB RAM, and a Solid-State Drive. In line

Table 5. Summary of the best values of hyperparameter for each of the models and tests.

Model	Hyperparameter	Testing range	Test	The best configuration within the testing range
SVR	Kernel function	'rbf', 'linear', 'polynomial'	#1	'rbf'
			#2	'rbf'
			#3	'rbf'
	C	0.1–10 000 (logarithmic)	#1	10 000
			#2	100
			#3	100
	epsilon	0.001–1 (logarithmic)	#1	0.01
			#2	0.01
			#3	0.01
XGBoost	Number of estimators	10–500	#1	70
			#2	490
			#3	490
	Maximum depth of trees	1–15	#1	4
			#2	5
			#3	5
	Learning rate	0.05–1	#1	0.35
			#2	0.25
			#3	0.25
KRR	Kernel function	'rbf', 'linear', 'polynomial'	#1	'polynomial'
			#2	'polynomial'
			#3	'polynomial'
	Alpha	0.001–100 000	#1	1
			#2	100
			#3	0.001

with table 6, it is apparent that SVR models not only are the most accurate ones, but also, they are the most stable models as their performance less fluctuated and their MAD value for both RV and RMSE is almost the least among the three AI algorithms. As an alternative option, the XGBoost is recommended as according to the information in table 6 it is the second accurate method for the same reasons of SVR. Finally, KRR is a simpler method that results in a good accuracy but not as high as SVR and XGBoost. However, subject to application and the required accuracy, the KRR model can also be used by the researchers.

Now, to illustrate a detailed performance of the developed models for prediction of the levitation and lateral forces, the part of the data that has not been utilized for training purposes (testing dataset) is implemented in the model and its predicted value is plotted along with the actual value. In this way, it can be seen how the model performs in estimating every single point. For this purpose, figure 13 is provided to demonstrate their predicted forces accuracy compared to the actual data. In these figures, static values for Z_{cp} , D_{sc} , h_{sc} , T and Z (specifically for test #1) were assumed and the variation of forces in relation to the position of the bulk is depicted. The corresponding values are provided alongside each of figure 13 (a), (b), and (c). As demonstrated by these figures, the model has accurately learned the data's pattern, resulting in the predicted and actual force values being remarkably close to each other.

Regarding the advances of this work, it is worth highlighting that this study presents significant advancements in

the characterization and modeling of MgB_2 superconducting bulks through the application of AI techniques. By developing and validating surrogate models, this research addresses critical gaps in traditional experimental methodologies, which are often costly and time-consuming. The key contributions of this work are:

1. We employed three advanced AI techniques—XGBoost, SVR, and KRR—to predict levitation and lateral forces between MgB_2 bulks and PM. These models demonstrated a worst-case accuracy scenario of 99.86%, providing an efficient and reliable alternative to finite element methods and experimental testing.
2. The AI models developed offer super-fast response times for estimating new data points, which is pivotal for real-time applications in magnetic levitation systems. This capability allows for quicker iterations during the design and testing phases of superconducting materials and devices.
3. The high accuracy of our AI models was validated against a comprehensive dataset obtained from rigorous experimental testing of MgB_2 bulks under various operational conditions. This validation underscores the reliability of AI techniques in replicating and extending experimental results.

The integration of AI into the study and development of superconducting materials offers numerous benefits to the community. Intelligent models based on AI techniques

Table 6. Summary of stability analysis for tests #1, #2, and #3.

Test	AI algorithm	Mean RV	MAD RV	Mean RMSE (N)	MAD RMSE (N)	Testing time (s)
#1	SVR	1.36×10^{-03}	1.94×10^{-04}	3.0414	5.0827	0.360
	XGBoost	3.00×10^{-03}	6.63×10^{-04}	4.4853	7.9706	0.018
	KRR	1.13×10^{-02}	1.34×10^{-03}	8.7704	16.5409	0.383
#2	SVR	6.66×10^{-04}	1.21×10^{-04}	0.1459	0.7083	0.425
	XGBoost	1.15×10^{-03}	1.61×10^{-04}	0.1918	0.6164	0.029
	KRR	3.36×10^{-02}	1.97×10^{-03}	1.0433	1.0866	0.397
#3	SVR	8.03×10^{-05}	1.00×10^{-05}	0.4405	0.1191	0.434
	XGBoost	3.58×10^{-04}	4.56×10^{-05}	0.9297	0.8594	0.026
	KRR	2.75×10^{-03}	2.89×10^{-04}	2.5759	4.1517	0.382

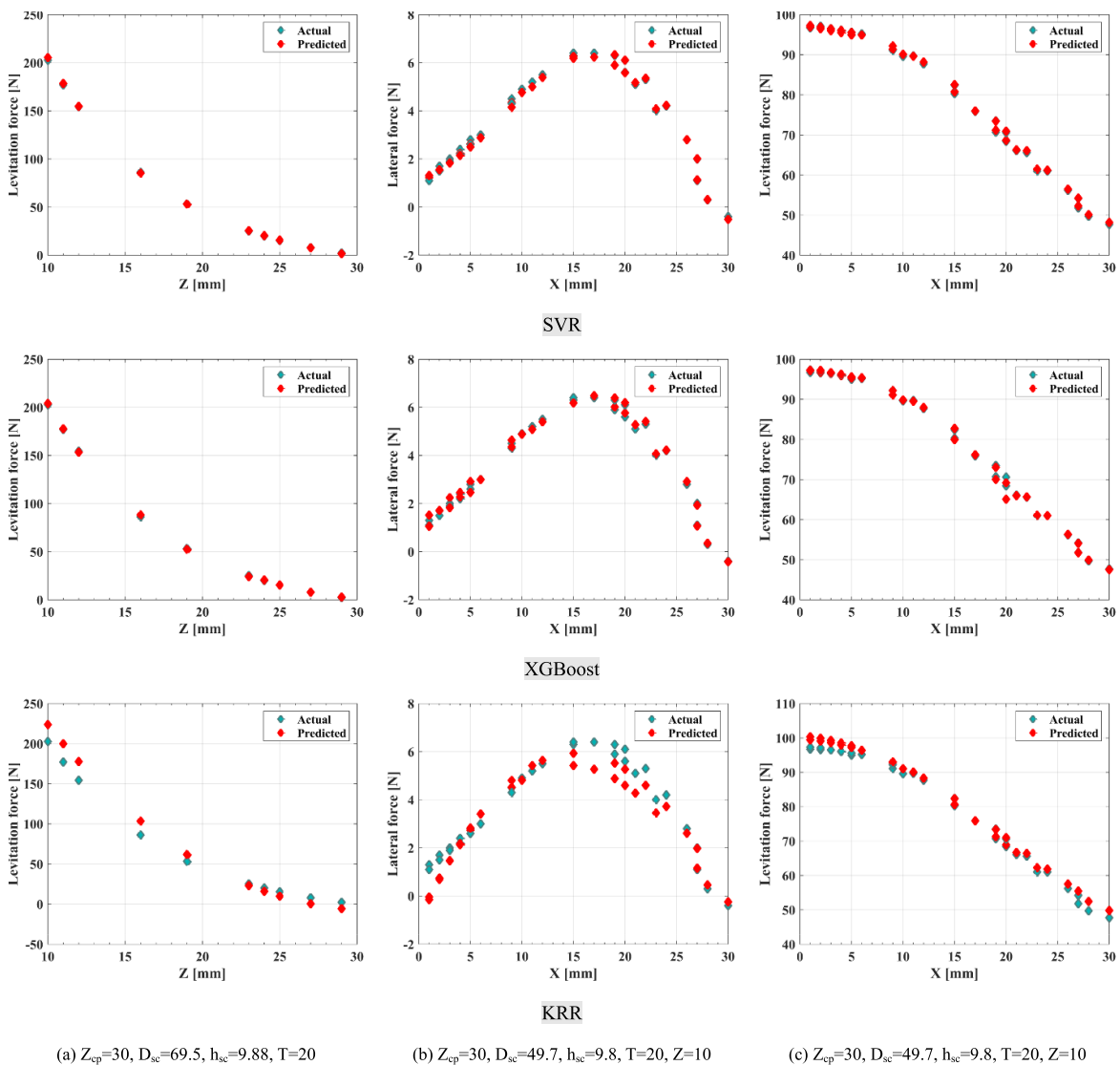


Figure 13. Predicted and actual value of SVR model for each of tests (a) #1, (b) #2, and (c) #3.

significantly reduce the time and resources required to evaluate and optimize superconducting materials, allowing for faster advancements in technology development. Also, their high predictive accuracy ensures that they can be reliably used to predict complex phenomena in superconducting systems, supporting the engineering of more robust and efficient devices. Moreover, referring to the fact that AI models benefit from scalability and versatility, they are adaptable to different types of superconductors and can be scaled to handle larger datasets and more complex system configurations, promoting broader application across various superconducting technologies and materials.

4.3.1. Discussion on extrapolation capabilities of AI models. One of the capabilities of AI models is the extrapolation of data beyond the range they have previously been trained on. In such cases, the model estimates values based on learned data patterns without having a prior knowledge of what to come. These cases are what the AI models will face in real-world after being trained and developed by experts in laboratories or companies. Although this paper does not primarily focus on this topic, we conducted two fairly complicated different extrapolations tests to evaluate the model's performance when applied to a new MgB₂ disk or new positions.

In the first scenario, we excluded the data from S1 in the training dataset for test #3 and selected XGBoost, known for its moderate accuracy among the three algorithms chosen in this paper, so, we did not want to have the best-case scenario with the best algorithm. We then used this data segment to test the trained model's performance. The results showed that the model could predict the levitational force of a new bulk sample with an RMSE of 6.725656, and an RV of 0.04575.

In the second scenario, we excluded the data for $x = 29$ and $x = 30$ for all samples, treating it as the testing dataset, and trained the model with the remaining data. In this scenario, the model exhibited excellent accuracy with an RMSE of 1.860467, and an RV of 0.00378.

These two scenarios prove the significant potential of AI methods for extrapolation and estimation in unseen out-of-range data conditions, which is usually the concern of many engineers and physicists in their real-time experimental studies.

5. Conclusion

Ten highly dense MgB₂ bulks of various dimensions were fabricated using SPS process. Magnetic levitation and guidance (lateral) force measurements were carried out at 20 K using a NdFeB magnet with a diameter of 70 mm and a thickness of 35 mm. These measurements served as input for training AI models, with the objective of rapidly and accurately correlating measurement data with simulation results to assess the levitation and lateral forces. In this paper, 9 models are developed based on three AI algorithms namely XGBoost, SVR, and KRR for prediction of levitation force in vertical movement (test #1), lateral (test #2) and levitation (test #3) forces in horizontal movement of the PM. Doing the sensitivity analysis on

the hyperparameters of the implemented algorithms ensures us that the models are at their optimum condition in which they can perform at highest accuracy. The key findings of this paper can be summarized as follows:

- SVR resulted in the highest accuracy amongst the three AI methods that are implemented in this paper for all the tests. It can estimate the levitation force in test #1 and #3 with an RV less than 1.36×10^{-03} and 8.03×10^{-05} , respectively. Also, it can predict lateral force in test #2 with an RV of 6.66×10^{-04} .
- Overall, the accuracy of prediction for test #3 is better than #2 and test #2 than #1. This can be due to the natural behavior and topology of the raw dataset used as inputs for AI models.
- The AI approach for estimating levitation and lateral forces of bulk superconductors showed an extensive goodness of fit to the experimental data collected from the explained tests.
- AI models have demonstrated their effectiveness as approaches for developing surrogate models to estimate magnetic levitation and lateral forces between MgB₂ bulks and a PM. Consequently, they can serve as cost-effective tools to advance the development and manufacturing of superconducting systems for strong and stable magnetic levitation.
- We speculate that the models we developed in this study are probably specific to the PM used in the experimental campaign. In fact, it is known that, physically speaking, the levitation and lateral forces depend on both the magnetic flux density and its gradient, which in turn depend on the PM. Since the approach of this study was intended to enhance the generalization capabilities of the models across different scenarios, we aim to include datapoints related to experiments involving different PMs and retrain the models to further extend their applicability in future studies.
- The developed AI models were tested for the cases of unseen and out-of-range data to demonstrate the excellent prediction performance of the model when it is used for extrapolations of any new cases. A very high accuracy achieved have firmly demonstrated such extrapolation capabilities for levitation and lateral force prediction of MgB₂ bulks.

Data availability statement

All data that support the findings of this study are included within the article (and any supplementary files).

Acknowledgments

For the purpose of open access, the author(s) has applied a Creative Commons Attribution (CC BY) license to any Author Accepted Manuscript version arising from this submission.

Yiteng Xing thanks the 'Conseil Régional-Normandie, France' for her Postdoc Grant-RIN Recherche "Emergent" from Normandy state (N° 21E04334).

ORCID iDs

Shahin Alipour Bonab  <https://orcid.org/0009-0002-8316-4336>


Yiteng Xing  <https://orcid.org/0000-0002-8818-7433>

Giacomo Russo  <https://orcid.org/0000-0002-2011-8423>

Antonio Morandi  <https://orcid.org/0000-0002-1845-4006>

Pierre Bernstein  <https://orcid.org/0000-0002-8104-2151>

Jacques Noudem  <https://orcid.org/0000-0002-8020-9095>

Mohammad Yazdani-Asrami  <https://orcid.org/0000-0002-7691-3485>

References

- [1] Durrell J H, Ainslie M D, Zhou D, Vanderbemden P, Bradshaw T, Speller S, Filipenko M and Cardwell D A 2018 Bulk superconductors: a roadmap to applications *Supercond. Sci. Technol.* **31** 103501
- [2] Werfel F N, Floegel-Delor U, Rothfeld R, Riedel T, Goebel B, Wippich D and Schirrmeister P 2012 Superconductor bearings, flywheels and transportation *Supercond. Sci. Technol.* **25** 014007
- [3] Deng Z et al 2016 A high-temperature superconducting maglev ring test line developed in Chengdu, China *IEEE Trans. Appl. Supercond.* **26** 1–8
- [4] Prikhna T et al 2013 Synthesis pressure–temperature effect on pinning in MgB₂-based superconductors *J. Supercond. Nov. Magn.* **26** 1569–76
- [5] Xing Y, Bernstein P, Muralidhar M and Noudem J 2023 Overview of spark plasma synthesis and sintering of MgB₂ superconductor *Supercond. Sci. Technol.* **36** 115005
- [6] Perini E, Bassani E, Giunchi G and Weisend J G 2010 The levitation characteristics of MgB₂ plates on tracks of permanent magnets *AIP Conf. Proc.* **1218** 261–8
- [7] Takahashi Y, Naito T, Nakamura T and Takahashi M 2021 Detection of 1H NMR signal in a trapped magnetic field of a compact tubular MgB₂ superconductor bulk *Supercond. Sci. Technol.* **34** 06LT02
- [8] Xing Y, Russo G, Ribani P L, Morandi A, Bernstein P, Rossit J, Lemonnier S, Delorme F and Noudem J 2024 Very strong levitation force and stability achieved with a large MgB₂ superconductor disc *Supercond. Sci. Technol.* **37** 02LT01
- [9] Mojarrad M, Farhoudian S and Mikheenko P 2022 Superconductivity and hydrogen economy: a roadmap to synergy *Energies* **15** 6138
- [10] Deng Z, Wang J, Zheng J, Lin Q, Zhang Y and Wang S 2009 Maglev performance of a double-layer bulk high temperature superconductor above a permanent magnet guideway *Supercond. Sci. Technol.* **22** 055003
- [11] Yazdani-Asrami M, Sadeghi A and Song W 2023 Ultra-fast surrogate model for magnetic field computation of a superconducting magnet using multi-layer artificial neural networks *J. Supercond. Nov. Magn.* **36** 575–86
- [12] Tsotsopoulou E, Karagiannis X, Papadopoulos T, Chrysochos A, Dyško A and Tzelepis D 2023 Protection scheme for multi-terminal HVDC system with superconducting cables based on artificial intelligence algorithms *Int. J. Electr. Power Energy Syst.* **149** 109037
- [13] Yazdani-Asrami M, Fang L, Pei X and Song W 2023 Smart fault detection of HTS coils using artificial intelligence techniques for large-scale superconducting electric transport applications *Supercond. Sci. Technol.* **36** 085021
- [14] Wu G and Yong H 2023 Estimation of critical current density of bulk superconductor with artificial neural network *Superconductivity* **7** 100055
- [15] Yazdani-Asrami M, Sadeghi A, Seyyedbarzegar S and Song W 2022 DC electro-magneto-mechanical characterization of 2G HTS tapes for superconducting cable in magnet system using artificial neural networks *IEEE Trans. Appl. Supercond.* **32** 1–10
- [16] Yazdani-Asrami M et al 2023 Roadmap on artificial intelligence and big data techniques for superconductivity *Supercond. Sci. Technol.* **36** 043501
- [17] Yazdani-Asrami M, Taghipour-Gorjikolaie M, Song W, Zhang M, Chakraborty S and Yuan W 2021 *Trans. Mag.* (available at: <https://hrcak.srce.hr/263818>) (Accessed 28 May 2024)
- [18] Zhu L, Wang Y, Meng Z and Wang T 2022 Critical current and n-value prediction of second-generation high temperature superconducting conductors considering the temperature-field dependence based on the back propagation neural network with encoder *Supercond. Sci. Technol.* **35** 104002
- [19] Yazdani-Asrami M, Taghipour-Gorjikolaie M, Song W, Zhang M and Yuan W 2020 Prediction of nonsinusoidal ac loss of superconducting tapes using artificial intelligence-based models *IEEE Access* **8** 207287–97
- [20] Yazdani-Asrami M 2023 Artificial intelligence, machine learning, deep learning, and big data techniques for the advancements of superconducting technology: a road to smarter and intelligent superconductivity *Supercond. Sci. Technol.* **36** 084001
- [21] Chen C, Xu J, Rong L, Ji W, Lin G and Sun Y 2022 Neural-network-state-observation-based adaptive inversion control method of maglev train *IEEE Trans. Veh. Technol.* **71** 3660–9
- [22] Ke Z, Deng Z, Chen Y, Yi H, Liu X, Wang L, Zhang P and Ren T 2022 Vibration states detection of HTS pinning maglev system based on deep learning algorithm *IEEE Trans. Appl. Supercond.* **32** 1–6
- [23] Pang P, Zheng J, Zhao Y, Xu L and Xian C 2024 Thermal-vibration correlation study for high-temperature superconducting maglev intelligent monitoring based on back propagation neural network analysis *Supercond. Sci. Technol.* **37** 025011
- [24] Ke Z, Liu X, Yi H, Jiang K, Wang L and Deng Z 2024 Nonlinear levitation-guidance coupling force prediction for HTS pinning maglev under arbitrary motion based on gated recurrent unit *IEEE Trans. Appl. Supercond.* **34** 1–6
- [25] Liu X, Ke Z, Chen Y and Deng Z 2022 The feasibility of designing a back propagation neural network to predict the levitation force of high-temperature superconducting magnetic levitation *Supercond. Sci. Technol.* **35** 044004
- [26] Noudem J G, Xing Y, Bernstein P, Retoux R, Higuchi M, Arvapalli S S, Muralidhar M and Murakami M 2020 Improvement of critical current density of MgB₂ bulk superconductor processed by spark plasma sintering *J. Am. Ceram. Soc.* **103** 6169–75
- [27] Dadiel J L et al 2021 Synthesis of dense MgB₂ superconductor via in situ and ex situ spark plasma sintering method *Materials* **14** 7395
- [28] Suarez M et al 2013 Challenges and opportunities for spark plasma sintering: a key technology for a new generation of materials *Sintering Applications (InTech)* (<https://doi.org/10.5772/53706>)
- [29] Morandi A et al 2018 The measurement and modeling of the levitation force between single-grain YBCO bulk superconductors and permanent magnets *IEEE Trans. Appl. Supercond.* **28** 1–10
- [30] Bernstein P, Xing Y, Noudem J, Morandi A, Ribani P L and Russo G 2024 The possible effect of surface barriers on the magnetic levitation of cylindrical superconductors *Supercond. Sci. Technol.* **37** 015019

- [31] Hull J R and Cansiz A 1999 Vertical and lateral forces between a permanent magnet and a high-temperature superconductor *J. Appl. Phys.* **86** 6396–404
- [32] Hsu C-W, Chang C-C and Lin C-J 2003 A practical guide to support vector classification (available at: www.csie.ntu.edu.tw/~cjlin/)
- [33] Platt J C 1999 Probabilistic outputs for support vector machines and comparisons to regularized likelihood methods (available at: www.researchgate.net/publication/2594015)
- [34] Cortes C, Vapnik V and Saitta L 1995 *Support-Vector Networks Editor* (Kluwer Academic Publishers)
- [35] Drucker H, Burges C, Kaufman L, Smola A and Vapnik V 1996 Support vector regression machines *Advances in Neural Information Processing Systems* vol 9 pp 155–61 (available at: https://proceedings.neurips.cc/paper_files/paper/1996/file/d38901788c533e8286cb6400b40b386d-Paper.pdf)
- [36] Platt J C 1998 Sequential minimal optimization: a fast algorithm for training support vector machines (available at: www.researchgate.net/publication/2624239)
- [37] Sadeghi A, Alipour Bonab S, Song W and Yazdani-Asrami M 2024 Intelligent estimation of critical current degradation in HTS tapes under repetitive overcurrent cycling for cryo-electric transportation applications *Mater. Today Phys.* **42** 101365
- [38] Theodoridis S and Koutroubas K 2009 *Pattern Recognition* 4th edn pp 1–961
- [39] Azzeh M, Elsheikh Y, Nassif A B and Angelis L 2023 Examining the performance of kernel methods for software defect prediction based on support vector machine *Sci. Comput. Program* **226** 102916
- [40] Zhang R, Li Y, Gui Y, Armaghani D J and Yari M 2024 A stacked multiple kernel support vector machine for blast induced flyrock prediction *Geohazard Mech.* **2** 37–48
- [41] Cao W, Liu Y, Mei H, Shang H and Yu Y 2023 Short-term district power load self-prediction based on improved XGBoost model *Eng. Appl. Artif. Intell.* **126** 106826
- [42] Chen T and Guestrin C 2016 *Proc. of the 22nd ACM SIGKDD Int. Conf. on Knowledge Discovery and Data Mining (San Francisco, California, USA)* pp 785–94
- [43] Li X, Ran Z, Zheng D, Hu C, Qin Z, Wang H, Wang Z and Li P 2024 Dynamic bond stress-slip relationship of steel reinforcing bars in concrete based on XGBoost algorithm *J. Build. Eng.* **84** 108368
- [44] Hoerl A E and Kennard R W 1970 Ridge regression: biased estimation for nonorthogonal problems *Technometrics* **12** 55–67
- [45] Russo G, Yazdani-Asrami M, Scheda R, Morandi A and Diciotti S 2022 Artificial intelligence-based models for reconstructing the critical current and index-value surfaces of HTS tapes *Supercond. Sci. Technol.* **35** 124002
- [46] Chen Z, Hu J, Qiu X and Jiang W 2022 Kernel ridge regression-based TV regularization for motion correction of dynamic MRI *Signal Process.* **197** 108559
- [47] Zheng Y, Ge Y, Muhsen S, Wang S, Elkamchouchi D H, Ali E and Ali H E 2023 New ridge regression, artificial neural networks and support vector machine for wind speed prediction *Adv. Eng. Softw.* **179** 103426
- [48] Exterkate P 2013 Model selection in kernel ridge regression *Comput. Stat. Data Anal.* **68** 1–16
- [49] Hazarika B B, Gupta D and Borah P 2021 An intuitionistic fuzzy kernel ridge regression classifier for binary classification *Appl. Soft. Comput.* **112** 107816
- [50] Ali M, Deo R C, Maraseni T and Downs N J 2019 Improving SPI-derived drought forecasts incorporating synoptic-scale climate indices in multi-phase multivariate empirical mode decomposition model hybridized with simulated annealing and kernel ridge regression algorithms *J. Hydrol.* **576** 164–84
- [51] Sanjika Devi R V, Bindu K R and Kurup D G 2022 Behavioral modeling and digital predistortion of RF power amplifiers based on time-delay kernel ridge regression *AEU—Int. J. Electron. Commun.* **152** 154239
- [52] You Y, Demmel J, Hsieh C J and Vuduc R 2018 Accurate, fast and scalable kernel ridge regression on parallel and distributed systems *Proc. Int. Conf. on Supercomputing, Association for Computing Machinery* pp 307–17
- [53] sklearn.svm.SVR—scikit-learn 1.4.0 documentation (available at: <https://scikit-learn.org/stable/modules/generated/sklearn.svm.SVR.html#sklearn.svm.SVR>) (Accessed 4 February 2024)
- [54] XGBoost Parameters—xgboost 2.0.3 documentation (available at: <https://xgboost.readthedocs.io/en/stable/parameter.html>) (Accessed 31 January 2024)